DRAFT VERSION SEPTEMBER 11, 2011
Preprint typeset using LaTeX style emulateapj v. 04/20/08

SLAC-PUB-14613

STATISTICS OF SATELLITE GALAXIES AROUND MILKY WAY-LIKE HOSTS

MICHAEL T. BUSHA[1,2], RISA H. WECHSLER[1,3], PETER S. BEHROOZI[1,3], BRIAN F. GERKE[1,3], ANATOLY A. KLYPIN[4], AND JOEL R. PRIMACK[5]

Draft version September 11, 2011

ABSTRACT

We calculate the probability that a Milky-Way-like halo in the standard cosmological model has the observed number of Magellanic Clouds (MCs). The statistics of the number of MCs in the ΛCDM model are in good agreement with observations of a large sample of SDSS galaxies. Under the sub-halo abundance matching assumption of a relationship with small scatter between galaxy *r*-band luminosities and halo internal velocities $v_{\rm max}$, we make detailed comparisons to similar measurements using SDSS DR7 data by Liu et al. (2010). Models and observational data give very similar probabilities for having zero, one, and two MC-like satellites. In both cases, Milky Way-luminosity hosts have just a $\sim 10\%$ chance of hosting two satellites similar to the Magellanic Clouds. In addition, we present a prediction for the probability for a host galaxy to have N_{sats} satellite galaxies as a function of the magnitudes of both the host and satellite. This probability and its scaling with host properties is significantly different from that of mass-selected objects because of scatter in the mass-luminosity relation and because of variations in the star formation efficiency with halo mass.

Subject headings: galaxies: dwarf, Magellanic Clouds, evolution — dark matter

1. INTRODUCTION

Understanding the satellite population of our own Milky Way galaxy is one of the outstanding problems in galaxy evolution studies today. Because these objects have weak gravitational potential wells, it is quite likely that different physical processes played a driving role in determining how such galaxies formed and evolved than for brighter, more massive objects. One manifestation of this is the well-known "missing satellites problem," which refers to the fact that the number of satellite galaxies predicted from simulations appears to be much higher than the number actually observed around the Milky Way (Klypin et al. 1999; Moore et al. 1999). One common way to address this problem has been to run simulations of individual objects using extremely high mass resolution. To date, roughly 10 of these ultra-high resolution N-body simulations have been run, which typically resolve individual Milky Way mass halos with upwards of 10^9 particles (Madau et al. 2008; Springel et al. 2008; Stadel et al. 2009).

The Magellanic Clouds (MCs) are a pair of well studied satellites of the Milky Way (MW) in the Southern Hemisphere with magnitudes $M_V = -18.5$ and -17.1 for the Large and Small Magellanic Clouds (LMC and SMC). While their large angular size makes detailed mass measurements somewhat difficult, observations constrain their maximum circular velocities to be around $v_{\rm max} \sim 60$ km s^{-1}(van den Bergh 2000; van der Marel et al. 2002; Stanimirović et al. 2004). Unlike the missing satellite problem, one common feature of these ultra-high resolution simulations is that they typically underpredict the number of massive satellites compared to the MCs in the MW (see, e.g., Figure 5 in Madau et al. 2008). Indeed, most of these high resolution halos contain no objects of similar mass to either of the two MCs. While this should hardly be taken as a serious problem since the handful of high resolution simulated halos does not constitute a statistical sample, it is important to understand how typical or atypical the Milky Way is, and whether or not not there is an "extra satellites" problem at high satellite masses within the modern Lambda Cold Dark Matter (ΛCDM) paradigm.

Because the MCs are relatively nearby and have been studied with high-precision instruments such as HST for some time, detailed 3-dimensional measurements of their velocities have been made (Kallivayalil et al. 2006b,a). Some of these studies have indicated that the Magellanic Clouds may be on their first orbit around the Milky Way (Besla et al. 2007; Busha et al. 2010); this may make such an extra satellite problem less worrisome if the presence of the Magellanic Clouds is a transient event. Regardless of the dynamical state of the Clouds, it is an important test of galaxy formation to understand the likelihood for MW-like systems to host massive satellite galaxies.

Recent developments have afforded us the possibility to address this problem in more detail with both observations and theoretical models. From the observational side, wide area surveys such as the Sloan Digital Sky Survey (SDSS York et al. 2000; Abazajian et al. 2009) have given us the ability to probe galaxy content for a large number of Milky Way-magnitude objects (Chen et al. 2006; James & Ivory 2010; Liu et al. 2010).

The main theoretical effort has been in populating dark matter halos with galaxies using semi-analytic methods and hydrodynamic simulations. Koposov et al. (2009) used a number of toy models to add galaxy properties to dark matter halos generated using a combination of Press-Schechter theory with semi-analytic models for tracking subhalo orbits (Zentner et al. 2005). They found that it was very difficult to model objects as bright as Magellanic clouds without allowing for an extremely high star formation efficiency. This finding extended the underprediction of high-mass subhalos to an under-

[1] Kavli Institute for Particle Astrophysics and Cosmology, Department of Physics, Stanford University, Stanford, CA, 94305, USA
mbusha@slac.stanford.edu, rwechsler@stanford.edu
[2] Institute for Theoretical Physics, University of Zurich, 8057 Zurich, Switzerland
[3] SLAC National Accelerator Laboratory, Menlo Park, CA, 94025, USA
[4] Astronomy Department, New Mexico State University, Las Cruces, NM, 88003, USA
[5] Department of Physics, University of California, Santa Cruz, CA 95064, USA

Submitted to Astrophysical Journal

KIPAC, SLAC National Accelerator Laboratory, 2575 Sand Hill Road, Menlo Park, CA 94025
Work supported in part by US Department of Energy contract DE-AC02-76SF00515.

prediction of luminous satellites, implying that the MW-MCs system is unusual. Similarly, Okamoto et al. (2010) explored a range of feedback models to add galaxies to some of the high resolution Aquarius halos (Springel et al. 2008). It was again difficult to readily reproduce halos with luminosities as bright as the MCs. Having looked in detail at a handful of simulated objects, however, this work indicates that there may be significant halo-to-halo scatter in the number of such massive objects. The idea of intrinsic scatter in the subhalo population was expanded on in Ishiyama et al. (2009a). While this work did not concentrate specifically on MC-like subhalos, they did consider the range in number of subhalos with $v_{max,sub}/v_{max,host} > 0.1$. This work showed an extremely large variation (20-60) in the number of such massive subhalos a galaxy-sized halos would host.

In contrast to the semi-analytic modeling just discussed, Libeskind et al. (2007) used hydrodynamic simulations to model the luminosity functions for the satellites around MW-like host halos. Their simulation identified 9 MW-like central galaxies and found that they, on average, have 1.6 satellites brighter than $M_V = -16$ and a third of them had satellites with luminosities comparable to the LMC.

The recent Millennium-II and Bolshoi simulations (Boylan-Kolchin et al. 2010; Klypin et al. 2010) have, for the first time, allowed us to probe cosmological volumes to understand the ΛCDM predictions for the satellite populations of MW-like halos. The properties of these simulations are summarized in Table 1. Boylan-Kolchin et al. (2010) (hereafter BK10) quantified the likelihood for $10^{12}\mathrm{M}_\odot$ halos to host massive satellite galaxies in the Millennium-II simulation, finding that subhalos similar to the MCs are quite rare. In this paper, we expand on this work by making similar measurements for the Bolshoi simulation, which used WMAP7 cosmological parameters, and using an abundance matching technique to make detailed comparisons between the Bolshoi predictions and the measurements from Liu et al. (2010). Our goal is to understand just how well ΛCDM reproduces the statistical properties of bright satellites.

Note that this is the reverse question from the one that was asked in a companion paper, Busha et al. (2010). That work assumed a satellite population and asked what the implications were for the properties of the host halo, including its mass. Here, we assume a host halo mass and ask about the implications for the subhalo population. There is no reason for both questions to give the same answer: while Busha et al. (2010) showed that a halo which hosts two MC-like satellites most likely has a mass near $1.2 \times 10^{12}\mathrm{M}_\odot$, there is no reason to assume that a typical $1.2 \times 10^{12}\mathrm{M}_\odot$ halo will have the MCs as satellites.

We begin by giving an overview of the Bolshoi simulation in §2, and then investigate the properties of massive dark matter satellites around dark matter host halos in §3, focusing on the mass ranges for hosts and satellites that are most relevant to the MW system. The analysis here is similar to that of BK10. In §4, we assign galaxy luminosities to our suite of dark matter halos and extend the results for a sample with similar selection cuts as for observations. In this way, we are able to make detailed comparisons to the observational work of (Liu et al. 2010, hereafter L10) concerning the satellite population around MW-magnitude galaxies. Section 4.4 gives the results of this analysis — see especially Figure 8. Finally, in §5, we expand this study to include the satellite population of a more general distribution of hosts, and §6 summarizes our conclusions. Throughout this paper, we adopt the convention $h = 0.7$ (the value that was used in the Bolshoi simulation) when reporting values from either simulations or observations.

2. SIMULATIONS

We use the dark matter halos identified in the Bolshoi simulation (Klypin et al. 2010; Trujillo-Gomez et al. 2010). This simulation modeled a 250 h^{-1}Mpc comoving box using cosmological parameters similar to those derived by WMAP7 (Komatsu et al. 2010): $\Omega_m = 0.27$, $\Omega_\Lambda = 0.73$, $\sigma_8 = 0.82$, $n = 0.95$, and $h = 0.7$. The simulation volume contains 2048^3 particles, each with a mass of $1.35 \times 10^8\ h^{-1}\mathrm{M}_\odot$ and was run using the ART code (Kravtsov et al. 1997). 180 snapshots from the simulation were saved and analyzed. One of the unique aspects of this simulation is the high level of spatial resolution employed, allowing objects to be resolved down to a physical scale of 1 h^{-1}kpc. This gives us excellent ability to track halos as they merge with and are disrupted by larger objects, allowing us to track them even as they pass near the core of the host halo. A summary of these simulation parameters is presented in Table 1. Because we discuss our work in the context of the BK10 results, we also present the same parameters for the Millennium II simulation (Boylan-Kolchin et al. 2009), on which the BK10 results were based.

Halos and subhalos were identified using the BDM algorithm (Klypin & Holtzman 1997). The algorithm identifies maxima in the density field and examines the neighboring region to identify bound particles. In this way, it treats both halos and subhalos identically. Subhalos are just identified as objects living within the virial radius of a larger objects. Because of the high level of mass and spatial resolution, BDM results in a halo catalog that is complete down to a maximum circular velocity $v_{\max} = 50$ km s^{-1}, where $v_{\max} = \max\left(\sqrt{GM(<r)/r}\right)$. This corresponds to a virial mass of roughly $10^{10}h^{-1}\mathrm{M}_\odot$. When BDM halos are identified, the ids of their 50 most bound particles are also stored to assist in producing merger trees.

As discussed in Section 4.2, in order to assign galaxy luminosities to dark matter halos, we need to track the histories of dark matter substructures. This is done using merger trees created from the 180 snapshots of the Bolshoi simulation. The detailed algorithm for creating the merger trees is described in Behroozi et al. (2010a). Briefly, the algorithm works by first linking halos across time steps by tracking the 50 most bound particles of each halo. Some halos will not have any of their 50 most bound particles identified at a later timestep (e.g., very massive objects in which the 50 most bound particles change rapidly through stochastic processes), while some will have their particles distributed to multiple halos. The algorithm corrects for this by running a simple N-body calculation on the locations and masses of all halos in the simulation to predict where each halo should wind up at the next time step. Using this information, it is possible to link halos across multiple time steps with very high accuracy.

3. SATELLITE STATISTICS FOR DARK MATTER SUBHALOS

We begin by investigating the properties of dark matter satellites around dark matter hosts in the Bolshoi simulation, focusing on the mass range for hosts and satellites that is relevant to the MW system. In §3.1, we consider trends with host halo mass, and in §3.2 we investigate trends with halo environment. We then consider the distribution of the satellite

TABLE 1
COMPARISON OF THE SIMULATION PARAMETERS FROM BOLSHOI (USED FOR THIS WORK) WITH THOSE OF THE MILLENNIUM II SIMULATION (USED IN BK10)

	Bolshoi	MSII
Box Size [Mpc]	357	143
N_P	2048^3	2160^3
$M_P[\mathrm{M}_\odot]$	1.9×10^8	9.8×10^6
h	0.7	0.73
Ω_M	0.27	0.25
σ_8	0.82	0.9
Force Resolution [kpc]	1.4 (proper)	1.4 (Plummer-equivalent softening)

number (§3.3). Finally, we extend this analysis to include a more observationally relevant selection based on galaxy luminosities in §4.

Because the mass resolution of the Bolshoi simulation creates a halo catalog complete down to 50 km s^{-1}, roughly equivalent to the lower bound of the mass of the MCs (van der Marel et al. 2002; Stanimirović et al. 2004; Harris & Zaritsky 2006), we begin by measuring the probability distribution for halos hosting N_{subs} subhalos with $v_{\max}$ larger than a given value. This measurement is made by identifying the virial radius of all distinct (non-subhalo) MW mass halos and counting the number of objects internal to their virial radii. We take the virial mass of the Milky Way to be $\log(M_{\rm vir}/\mathrm{M}_\odot) = 12.08\pm0.12$ ($M_{\rm vir} = 1.2\times10^{12}\mathrm{M}_\odot$), the mass measured in Busha et al. (2010), which is consistent with most results in the literature (Battaglia et al. 2005; Dehnen et al. 2006; Smith et al. 2007; Xue et al. 2008). This results in 36,000 MW analogs found in the Bolshoi volume. We present the resulting probability distribution of satellite counts as the colored points in the left panel of Figure 1. Here, the different colors represent different thresholds for satellite $v_{\max}$: red, green, and blue represent all satellites with $v_{\max} > 50$, 60, and 70 km s^{-1}. Error bars were calculated using the bootstrap method and represent 95% confidence intervals.

From Figure 1, we can immediately see that the likelihood of hosting multiple satellites is somewhat low. For satellites with $v_{\max}$ greater than 50 km s^{-1}, roughly 30% of simulated hosts contain one or more subhalos and just 8% have two or more. These numbers are in excellent agreement with the work of BK10, who performed a similar analysis on the Millennium II simulation, which was run using a different N-body code in a WMAP1 cosmology and with a very different subhalo identification algorithm. The probability of hosting multiple satellites drops precipitously with increasing satellite mass; e.g., the probability of a halo hosting two subhalos larger than $v_{\max}$ = 70km s^{-1} is just 1%.

For comparison, the black points in Figure 1 represent measurements from Liu et al. (2010), who measured the probability distribution for finding MC-luminosity satellites within 250 kpc around isolated MW-luminosity galaxies (the mean virial radius of our sample). We only plot these measurements out to N_{subs} = 3 because, for a 250 kpc aperture, uncertainties from their background subtraction become extremely large for higher (lower probability) values of N_{subs}. Here, the agreement for satellites larger than 50 km s^{-1}is striking, indicating that CDM can reproduce the statistics of MCs. We must, however, be careful about over-interpreting this result. In particular, their selection criteria are very different from our mass selection. We will return to this in §4.4 where we make a comparison directly to similarly selected samples.

By comparison with the Bolshoi simulation, the existence of two satellites with $v_{\max}$ larger than 50km s^{-1} makes the MW almost a 2σ outlier. Understanding whether anything other than random chance is responsible for putting the MW in this slightly rare regime motivates further investigation into which other properties may correlate with satellite abundance. In particular, we investigate the correlation of the number of subhalos with host mass and environment.

3.1. *Mass dependence*

The correlation between subhalo abundance and host mass has been well studied (Zentner & Bullock 2003; Diemand et al. 2004; Gao et al. 2004; Zentner et al. 2005; Klypin et al. 2010). These studies have all found that, when scaled in units of $\mu = M_{sub}/M_{host}$, larger halos contain more subhalos above a given μ than do smaller ones. This is the expected result from the hierarchical merging picture of CDM, in which larger objects grow through the merging of smaller objects and therefore form later (Blumenthal et al. 1984; Lacey & Cole 1993). This later formation has a two-fold impact: it reduces the amount of time available to tidally strip a subhalo, and lowers the host concentration, further reducing the ability of a host to tidally strip its subhalos (Wechsler et al. 2002; Busha et al. 2007). Motivated by this, we present the abundance of LMC and SMC-mass subhalos for the 27,000 Bolshoi halos with $M_{\rm vir} = 2.6\pm0.9\times10^{12}\mathrm{M}_\odot$. The results can be seen in Figure 1. Here, the left panel shows the results for selecting hosts with $M_{\rm vir} = 0.8-1.7\times10^{12}\mathrm{M}_\odot$, while the right panel shows a mass range $M_{\rm vir} = 1.7-3.4\times10^{12}\mathrm{M}_\odot$.

For the more massive $M_{\rm vir}\sim2.6\times10^{12}\mathrm{M}_\odot$ halos, the cumulative probability of hosting two or more 50 km s^{-1} halos increases by a factor of 3 compared to the $1.2\times10^{12}\mathrm{M}_\odot$ objects (from 8% to 26%), while jumping by a factor of 6 for 70km s^{-1} subhalos (from 1% to nearly 6%). We emphasize that this is not a contradiction with the results of Busha et al. (2010), which found that a halo with exactly two MC-like subhalos was likely to have mass $1.2\times10^{12}\mathrm{M}_\odot$. While the fraction of more massive halos hosting two MC-like subhalos is larger, the steep slope of the mass function means that there are many more lower-mass halos. Additionally, aside from just considering $v_{\max}$, Busha et al. (2010) selected halos with satellites like the MCs in terms of location and three-dimensional velocity, properties not considered in the present analysis.

Again, these results are in excellent agreement with the work of BK10. While such an agreement is generally expected from pure collisionless N-body simulations, such agreement is not as trivial as it may appear. While the present work uses results from the Bolshoi simulation, run using the adaptive refinement ART code and the BDM halo finder, BK10 used the Millennium-II simulation run with the TreePM code Gadget-2 with substructures identified using the Subfind algorithm (Springel et al. 2001). Additionally, in both cases, we are concerned with subhalos close to the mass-limit for the simulations. Thus, the close agreement between these two works suggests that numerical effects in the simulations are well understood at this level.

3.2. *Environmental dependence*

Beyond simple host mass dependence, the size of the cosmological volume modeled by the Bolshoi simulation allows

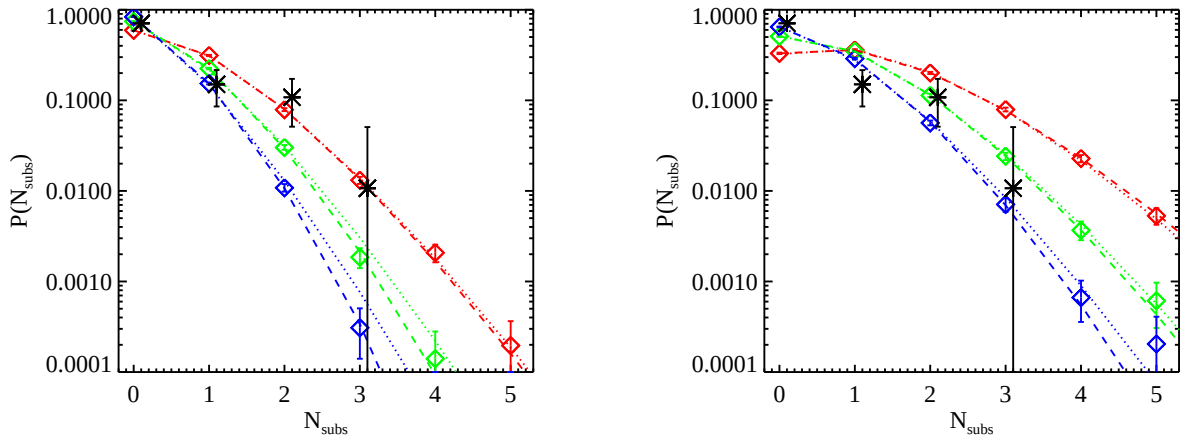

FIG. 1.— The probability distribution for the abundance of MC-like satellites around MW-mass hosts in simulations (colored diamonds). The left panel shows the results for hosts in a mass bin of $M_{\rm vir} = 1.2 \pm 0.3 \times 10^{12} {\rm M}_\odot$; the right panel shows results for hosts in a mass bin of $M_{\rm vir} = 2.6 \pm 0.4 \times 10^{12} {\rm M}_\odot$. In both cases, the red, green, and blue distributions correspond to the number of satellites with $v_{\rm max} > 50$km s^{-1}, $v_{\rm max} > 60$km s^{-1}, and $v_{\rm max} > 70$km s^{-1}, respectively. Dashed lines show the best-fit negative binomial distribution, and dotted lines show the best-fit Poisson distribution. In both panels, the black points show the observational result of Liu et al. (2010) for the number of satellites within 250 kpc around isolated MW-luminous galaxies.

us to perform further detailed studies on properties impacting the satellite abundance distribution. Here, we quantify the environmental dependence of the subhalo population by splitting the sample on local density, defined by

$$\delta_{h,r} = \frac{\rho_{h,r} - \bar{\rho}_h}{\bar{\rho}_h}, \tag{1}$$

where $\rho_{h,r}$ is the Eulerian density of dark matter contained in halos larger than $M_{\rm vir} = 2 \times 10^{11} {\rm M}_\odot$ (roughly 1000 particles in Bolshoi) defined in a sphere of size r. In the present analysis, we take $r = 1.0h^{-1}$Mpc; we have performed similar analysis on a range of scales and find this to be the range where the galaxy halo distribution is the most sensitive to the presence of massive satellites.

We compare the distribution $P(N_{subs})$ for halos in the top and bottom quartile distributions to the mean relation in Figure 2. There is a clear systematic trend: halos living in overdense regions (red points) are more likely to host massive subhalos than those in underdense regions (blue points). This is likely due to the fact that halos in denser environments live in more biased regions, where smaller density perturbations are amplified, making it easier for smaller halos to form and accrete onto intermediate mass hosts. This makes the deviations from the mean relation in Figure 2 a potentially observable manifestation of assembly bias, which posits that the properties of a given halo may be determined by properties other than mass, such as the halo environment.

Selecting for objects in a dense environment increases by almost 25% the probability of having $N_{subs} = 2$ or more, from 9% to just over 11%; this effect becomes stronger for larger values of N_{subs}. The Milky Way is somewhat overdense on this scale, having a massive companion, M31, as well as a number of surrounding dwarf galaxies. Recent estimates put the total mass of the local group at roughly $5 \times 10^{12} {\rm M}_\odot$ (Li et al. 2009), solidly in a dense environment on the ~ 1 Mpc scale. Even if we ignore the contribution to the local density from all neighboring objects except M31, the MW lies close to the top quartile of our measured local density distribution in Bolshoi on a ~ 1 Mpc scale. We can begin to directly quantify the impact of such a massive neighbor on the subhalo population by identifying MW-mass halos which have M31-like neighbors

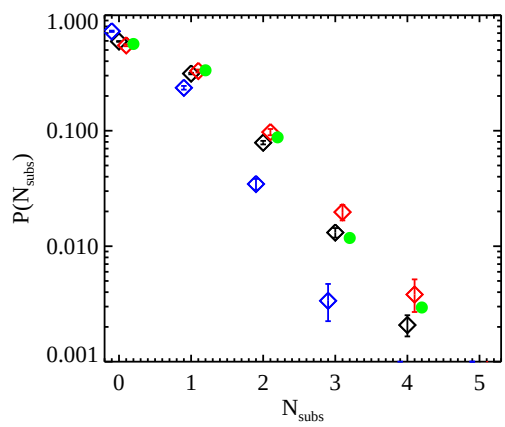

FIG. 2.— The probability that a $1.2 \times 10^{12} {\rm M}_\odot$ halo hosts N_{subs} subhalos with $v_{\rm max} > 50$km s^{-1}, split by local host density. The black points represent all halos, while the red and blue points represent the most overdense and underdense quartiles, respectively. Green circles represent MW-mass halos that were selected to have M31-mass neighbors.

with $M_{\rm vir} = (1-3) \times 10^{12} {\rm M}_\odot$ at a distance of 700-900 kpc. These systems are represented by the green circles in Figure 2, which have a $N_{subs} = 2$ probability enhanced by 2σ relative to the full sample. Thus, the local environment around the MW, which is dominated by the presence of M31, boosts the chance of seeing the Magellanic Clouds in the Milky Way.

3.3. *Probability distributions*

As an extension of the trends shown in Figure 1, it is useful to generalize these results to arbitrary host and subhalo masses by fitting the probability distribution. A Poisson distribution seems to be the most natural assumption, and has been found previously in the literature (e.g., Kravtsov et al. 2004). Deviations from a Poisson distribution can be quantified by the calculation of the second moment, α_2, where

$$\alpha_2 = \frac{\langle N(N-1) \rangle}{\langle N \rangle^2}. \tag{2}$$

For a Poisson distribution, $\alpha_2 = 1$. While studies have found some evidence for a deviation from Poisson, with $\alpha_2 > 1$ (Kravtsov et al. 2004; Wetzel & White 2010), the distribution has been more fully quantified by BK10. This work found that the distribution could be much better modeled using a negative binomial distribution,

$$P(N|r,p) = \frac{\Gamma(N+r)}{\Gamma(r)\Gamma(N+1)} p^r (1-p)^N \quad (3)$$

where

$$p = \frac{1}{1+(\alpha_2^2-1)\langle N\rangle}, \quad r = \frac{1}{\alpha_2^2-1}, \quad (4)$$

although they note that a Poisson distribution is a reasonable fit when $\langle N\rangle$ is low, such as the case of the MCs. We plot fits to both a Poisson and a negative binomial distribution to our measurements as the dotted and dashed lines in Figure 1. We again see that, because $\langle N\rangle < 1$, the Poisson distribution provides a reasonable fit, while the negative binomial distribution fit is excellent (at the expense of adding an additional parameter).[6] Our results confirm those of BK10, in that the distribution becomes significantly more non-Poisson for larger values of $\langle N\rangle$.

As a final comparison of the Bolshoi halos to previous work in the literature, we plot in Figure 3 the trends of $\langle N\rangle$ (top panel, similar information to Figure 15 in Klypin et al. 2010) and α_2 (bottom panel) with mass ratio $v_{acc,sub}/v_{max,host}$ for a range of host masses. Here, $v_{acc,sub}$ is the maximum circular velocity, v_{max}, that the subhalo had at the epoch of accretion. As seen in the top panel, the value for $\langle N\rangle$ scales almost self-similarly, but with a slight increase in overall normalization as has been previously noted in the literature (Gao et al. 2004; Klypin et al. 2010; Gao et al. 2010), indicating that more massive halos contain somewhat more subhalos, proportionally, than lower mass halos.

More interesting is the trend in α_2 with mass, shown in the lower panel of Figure 3. Here we see evidence that, for subhalos with $v_{acc,sub}/v_{max,host} \gtrsim 0.25$, self-similarity breaks down much more significantly, where lower-mass hosts tend to have systematically higher values of α_2, which implies increased scatter beyond Poisson statistics. There are a number of possible explanations for this trend; it may be due to the fact that lower mass objects exist in a wider range of environments than higher mass halos. As shown earlier in Figure 2, the immediate environment surrounding a halo can have a significant impact on its subhalo population. High-mass halos always form in regions of high bias, meaning that the environmental impact on a high mass object's subhalo population is minimized. Low-mass objects are able to form in both biased and unbiased regions and in regions near to higher mass halos, creating a larger scatter in their subhalo populations. While not shown, we have made analogous plots to Figure 2 for hosts of higher mass and confirm that these objects typically display weaker environmental dependence in their subhalo populations.

It is also interesting to note that previous studies, in particular Kravtsov et al. (2004) and BK10, have not seen such a trend. There are a number of possible explanations for this, which include the improved $1h^{-1}$kpc force resolution and

[6] Note that, when calculating these fits, it is possible to either calculate $\langle N\rangle$ and α directly from the data, or to treat them as free parameters to the fitting algorithm. However, in practice the differences in resulting parameters are less than 5%.

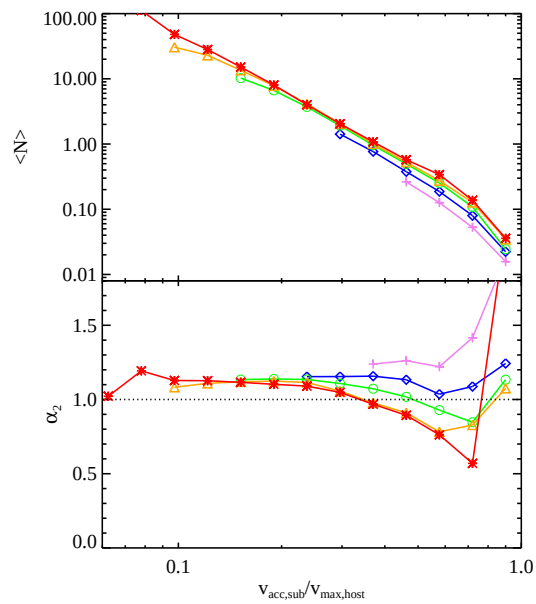

FIG. 3.— *Top Panel:* The trend of $\langle N\rangle$ for the v_{acc} distribution function for hosts of varying masses. This is equivalent to the subhalo mass function. Magenta pluses, blue diamonds, green circles, and red triangles represent hosts with $v_{\rm max}$ = 200, 300, 600, and 1000 km s^{-1}, respectively. *Bottom Panel:* The trend of the scatter in the distribution of the number of subhalos above a mass threshold. The dashed line represents $\alpha_2 = 1$, where the negative binomial distribution reduces to Poisson.

$(250h^{-1}\mathrm{Mpc})^3$ volume of the Bolshoi simulation, which allows for both better statistics and more accurate tracking of subhalos as they orbit around their hosts. The increased volume of Bolshoi is particularly important if the trend is driven by halo environment, since a larger volume is necessary to probe a full range of environments. Hints of this trend, however, can be noticed in Figure 9 of BK10. While not shown, nearly identical trends in $\langle N\rangle$ and α_2 persist if we consider the mass ratio $v_{max,sub}/v_{max,host}$, using the maximum circular velocity of the subhalo at $z = 0$ instead of at the time of accretion.

To summarize, in this section, we have shown that satellites comparable in size to the LMC and SMC are relatively rare in MW mass objects, occurring in roughly 9% of the potential hosts. Their abundance is dependent on a number of host properties, such as the host mass and environment. The latter can provide a boost at the 25% level. The proximity of M31 puts the Milky Way in a higher density environment, which increases the likelihood of an LMC/SMC pair to 12%. Finally, it was shown that for massive subhalos, the scatter in the expected number of subhalos systematically decreases with increasing host mass. This may be related to the environmental variations previously observed; lower mass halos are able to form in a wider range of environments than higher mass objects. In the next section, we turn to the task of comparing our simulation results with observations from the SDSS, which requires the adoption of an algorithm for adding magnitudes to simulated galaxies.

4. SATELLITE STATISTICS FOR GALAXIES

We turn next to a detailed comparison of these results with observational measurements. The classical satellite galaxies around the MW have been well-studied, with the SMC and LMC being the only satellites brighter than $M_V = -16$. Indeed, the next brightest object, Sagittarius, with $M_V = -13.1$,

is roughly 3 magnitudes dimmer than the SMC. Motivated by this, we search for the distribution of the number of satellites of $M_V \leq -16$ in other galaxies, both simulated and real. In order to distinguish the results in this section from the previous sections, we adopt the formalism where N_{sats} refers to the number of satellite galaxies around a host, identified based on their luminosities. This contrasts with mass-selected dark matter subhalos, which we characterized in the previous sections using the nomenclature N_{subs}.

4.1. *The Observational Sample*

Our recent companion paper (Liu et al. 2010, hereafter, L10) studied the population of such LMC and SMC-luminosity objects in the SDSS. Here, MW analogs were identified in the SDSS main sample by locating objects with absolute magnitudes $M_r = -21.2 \pm 0.2$ with no brighter companions within a line-of-sight cylinder of radius 500 kpc and length 28 Mpc (corresponding to a redshift of ± 1000 km s^{-1}).[7] The abundance of satellite galaxies was then measured by calculating the likelihood of having N_{sats} neighbors in the photometric sample with apparent magnitudes 2-4 dimmer in a fixed 150 kpc aperture. While we discuss details of their method below, our goal here is to compare our simulated results to their observational constraints.

4.2. *Modeling Galaxy Luminosities*

Because internal kinematics are difficult to measure observationally for dwarfs outside the Local Group, the observations of L10 cannot be directly compared to the results from the previous section, which determined abundances based on the v_{max} of the satellites. Instead, we employ a SubHalo Abundance Matching (SHAM) algorithm to our simulation to map magnitudes onto dark matter halos (Kravtsov et al. 2004; Conroy et al. 2006; Wetzel & White 2010; Klypin et al. 2010; Behroozi et al. 2010b). Here, luminosities are assigned by matching the number density of observed objects brighter than a given luminosity with the number density of simulated objects greater than a given $v_{\rm max}$. For subhalos, $v_{\rm max}$ at the time of accretion is used instead of the present $v_{\rm max}(z = 0)$. We also impose a log-normal scatter between halo mass and luminosity. In our base model, we assume a scatter of 0.16 dex, consistent with constraints on larger group and cluster mass objects (More et al. 2009; Behroozi et al. 2010b).

This algorithm has been shown to be extremely successful in matching several statistical properties of the galaxy distribution, including the luminosity dependence and redshift scaling of the two-point galaxy correlation function for galaxies brighter than $M_r < -19$ (Conroy et al. 2006), the galaxy-mass correlation function (Tasitsiomi et al. 2004), and galaxy three point statistics (Marín et al. 2008). Klypin et al. (2010) have shown that a similar procedure can simultaneously match the luminosity function and the Tully-Fisher relation locally.

Here, we match halos directly to the binned r-band luminosity function in the local Universe as measured by Blanton et al. (2005) for galaxies with $M_r < -12.8$. While there is some uncertainty in these measurements depending on the detailed surface brightness correction, the objects we are interested in here are bright enough that this effect is unimportant. This luminosity function also reproduces the more recent number densities measured in SDSS DR7 (Zehavi et al. 2010) down to $M_r \sim -17$. The results of this procedure are shown in Figure 4. Here, the red line shows the relation between $v_{max,acc}$ and magnitude, while the blue points show $v_{\rm max}$ at $z = 0$. The systematic movement to lower $v_{\rm max}$ for many objects is due to tidal stripping of subhalos. The resulting simulated catalog has a distribution of galaxies that is complete down to $M_r = -15.3$. Note that our pure-abundance matching measurements from Figure 4 gives most likely mass estimates for the LMC and SMC to be $v_{\rm max} = 85 \pm 6$ and 65 ± 6km s^{-1}, respectively. However, as shown in Trujillo-Gomez et al. (2010), ignoring the effects of baryons likely increases the maximum circular velocity by roughly 10% (see their Figure 5), bringing our SHAM mass estimates into excellent agreement with the observations

Using luminosities assigned in this way, we now make measurements analogous to those of L10. We select for MW candidates in the same way as L10. First, we make a mock lightcone by taking the $z = 0$ SHAM catalog of the Bolshoi simulation, placing an observer at the center of the box, and adding redshift space distortions. We passively evolve galaxy magnitudes to the appropriate redshift using the SDSS constraint $M_r(z) = M_r(z = 0.1) + Q(0.1 - 1)$, with $Q = -1.3$ (Blanton et al. 2003). We then identify all isolated objects by selecting halos with $M_r = -21.2 \pm 0.2$ (the upper grey band in Figure 4 and excluding objects having a brighter neighbor in a cylinder of radius 500 kpc and length 28 Mpc. The resulting $v_{\rm max}$ distribution is shown in Figure 5. This distribution is somewhat lower than the best current estimates for the maximum rotational velocity of the MW, $v_{rot} = 220$ km s^{-1}(Xue et al. 2008; Gnedin et al. 2010). This difference should not be surprising since $v_{\rm max}$ includes only the dark matter, while v_{rot} is the total rotational speed of an actual halo that includes the full impact of baryons. Further, Trujillo-Gomez et al. (2010) have shown that, because the Milky Way sits near the peak of the star formation efficiency, baryons play a significant role in determining the circular velocity profile of MW mass halos, resulting in a value of $v_{\rm max}$ that is underestimated in dark matter-only simulations. However, the virial mass of the galaxies that pass our MW selection peaks at $1.3 \times 10^{12} M_\odot$, in excellent agreement with the estimated MW mass from Busha et al. (2010).

We select for MC-analogs using a method similar to L10, identifying all satellites within the virial radius of our MW analogs that are 2-4 magnitudes dimmer (lower grey band in Figure 4). The most likely $v_{\rm max}$ values for our MC analogs are ~ 80 and ~ 70 km s^{-1}, in agreement with the 1-σ constraints from observations(van der Marel et al. 2002; Stanimirović et al. 2004; Harris & Zaritsky 2006).

4.3. *The Definitions of a Satellite*

Before presenting detailed comparisons between the L10 observational data and our model, we note that the definition of a "satellite" differs between the two analyses. Because L10 used a photometric sample with hosts selected on luminosity and no spectroscopy for their satellites, the number of satellites was defined as the number of photometric pairs around a host. Specifically, they identified isolated MW-luminosity galaxies in the SDSS spectroscopic sample and counted the number of photometric pairs with $\Delta m_r = 2 - 4$ within a fixed angular separation, nominally taken to be 150 kpc. They then applied a background subtraction to account for projection effects and correlated structures. While our SHAM catalog will let us select isolated host objects in an analogous way, because modeling the full distribution of galaxy apparent mag-

[7] The value for the r-band absolute magnitudes was determined using the K-correction code of Blanton & Roweis (2007) on a sample population of 500,000 SDSS galaxies.

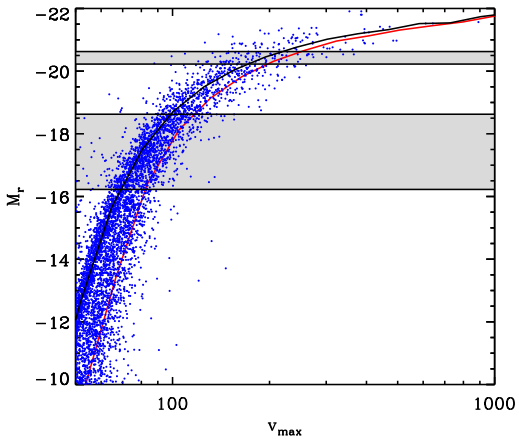

FIG. 4.— The relation between magnitude and v_{max} for simulated halos+SHAM. The red line represents the relation between M_r and v_{acc}, the maximum circular velocity at the time of accretion, which was used to select the magnitude. The black curve and blue points show the relation the between magnitude and $v_{\rm max}$ at $z = 0$ (as opposed to v_{acc}). The upper grey band shows our magnitude-criteria for selecting Milky Way-like hosts, while the lower gray band represents our range for selecting Magellanic Cloud-like satellites.

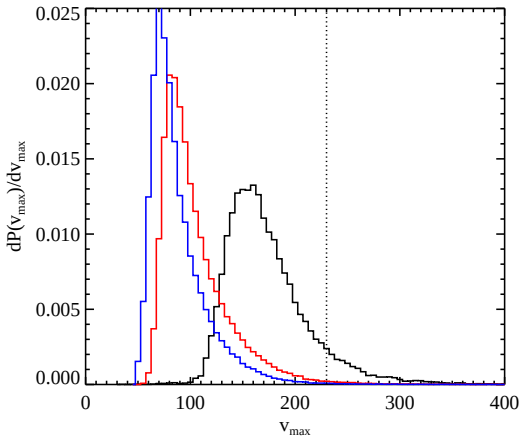

FIG. 5.— The distribution of v_{max} for simulated galaxies, as selected by luminosity. The black histogram represents galaxies that pass our Milky Way selection, with $M_r = -21.2 \pm 0.2$, while the blue and red histograms represent v_{max} and v_{acc} for our Magellanic Cloud-like subhalos that are 2-4 magnitudes dimmer than their hosts. The dotted line shows the preferred value for v_{vir} of the MW.

nitudes is beyond the scope of our model, we do not perform an identical calculation. Instead, we can select an appropriate definition of a satellite galaxy to mimic the observational effects.

L10 presented two methods for background subtraction, which were used to calculate the number of satellites around a host galaxy. The first, which we refer to as isotropic subtraction, assumed that background objects had, on average, no dependence on position (implicitly ignoring the impact of correlated structures), to calculate an average background for their entire host population. Using this assumption, it is possible to calculate the average background to very high statistical accuracy. Their second method, which we refer to as annulus subtraction, measured the background object counts around each galaxy by considering the region just outside the projected region surrounding the galaxy. For completeness, we

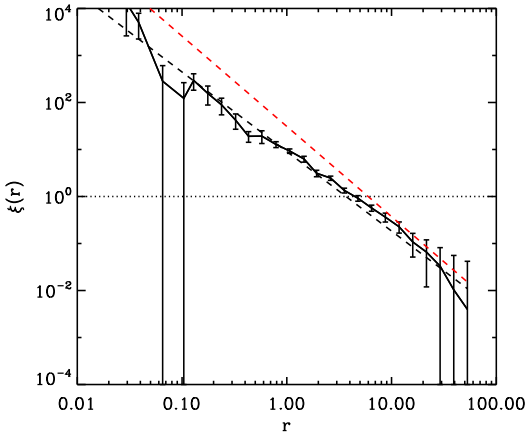

FIG. 6.— The 3D cross-correlation function, $\xi(r)_{\rm MW-MC}$, between Milky Way like hosts and all LMC and SMC magnitude satellite galaxies. The black dashed line represents a power-law fit to $\xi(r)$. For reference, the dotted red line denotes the auto-correlation between galaxies with $-21 < M_r - 5\log(h) = -20$ in SDSS DR7 as measured in Zehavi et al. (2010).

make comparisons to both methods.

Because it removes the effects of correlated structures, comparison to the annulus subtraction method of L10 is straightforward. We define as a satellite galaxy any object within the appropriate spherical volume (taken to be 150 kpc in L10) that has an absolute magnitude that is 2-4 mag dimmer than its host. To compare to the isotropic subtraction method, which neglects the impact of correlated structures along the line of sight (see Section 3.2 of L10 for further discussion) requires additional modeling. We account for this by defining a satellite to be any object inside a cylinder of radius 150 kpc and length r_0, where r_0 is the correlation scale for the Milky Way host-satellite analog.

This cross-correlation function between MW-luminous galaxies and objects 2-4 magnitudes dimmer is plotted in figure 6, and is well fit by a power law,

$$\xi(r) = (r/r_0)^{-\gamma} \tag{5}$$

with $r_0 = 5.3$ Mpc and $\gamma = 1.7$, with a similar correlation length to measurements for all galaxies of MW-like magnitudes inferred from Zehavi et al. (2010). These authors measured $r_0 = 5.98$ Mpc/h and $\gamma = 1.9$ for the autocorrelation function of galaxies with $M_r = -20.7$ to -21.7. We therefore consider a cylinder with radius 150 kpc and length 5.3 Mpc (the correlation length) to be the appropriate aperture for satellite selection to compare to the isotropic background subtraction of L10.

Coincidentally, this correlation scale is very similar to the size of the expected redshift-space distortions. Evrard et al. (2008) showed that a $\sim 10^{12} M_\odot$ halo has a typical velocity dispersion of 125 km s^{-1}; at $z = 0.08$, where the bulk of our simulated halos live, this corresponds to a 3.7 Mpc spread due to the redshifts of the satellite population. A cylinder of this length thus represents the most accurate measurements one could make for the number of satellites around a host using spectroscopic data (without including some sort of additional background subtraction).

In Figure 7 we compare the $P(N_{subs})$ distribution for four different satellite definitions: spherical and cylindrical apertures (which correspond to the L10 results using their annulus and isotropic background subtractions methods, respectively) as well as selecting satellites based on $v_{\rm max}$ and abundance-

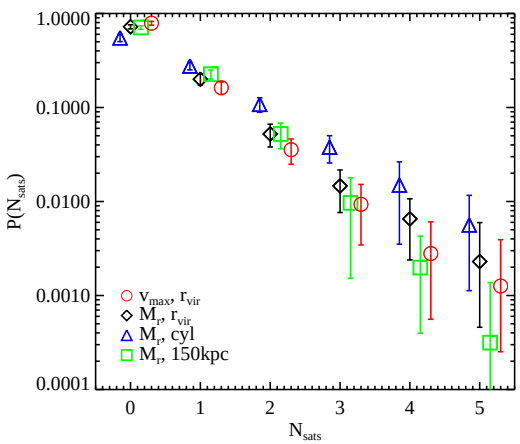

FIG. 7.— The probability of having N_{sats} LMC and SMC-type objects in simulations based on SHAM and v_{max} for various satellite definitions. Red circles count objects with $v_{max} > 50$ km s^{-1}within the virial radius; the black diamonds, blue triangles, and green boxes count objects 2-4 magnitudes dimmer than their host using a SHAM model with 0.16 dex scatter. The black diamonds were calculated using all objects inside the virial radius. The blue triangles and green boxes are equivalent to the isotropic and annulus background subtractions used in L10: a cylindrical aperture of radius 150 kpc and length 5.3 Mpc (blue triangles), and a fixed 150 kpc spherical aperture (green boxes).

matched magnitude. Here, the red circles consider subhalos within the virial radius of their host that have $v_{max} = 50-80$km s^{-1}. The black diamonds, blue triangles, and green boxes all use magnitude-selected satellites, counting objects 2-4 magnitudes dimmer than their host using the aforementioned SHAM model with cuts analogous to the observational criterion of L10. The red diamonds represent the "correct" number of satellites, using all objects inside the virial radius, The blue triangles use a cylindrical aperture, analogous to the isotropic background subtraction of L10, while the green boxes use a spherical aperture, equivalent to the annulus subtraction method of L10. All error bars were calculated using the jackknife method with 10 sub-regions.

A number of trends are readily apparent for the relations in Figure 7. First, there is generally good agreement between the $P(N_{subs})$ distribution for objects based on $v_{\rm max}$ (red circles) with our SHAM magnitudes (black diamonds). This is to be expected if SHAM preserves the observed mass-luminosity relation in this regime, something that will only happen if an appropriate mass function is used. It is also interesting to note that our calculations for the cylindrical aperture (blue triangles) always lie above the other measurements for $N_{subs} \geq 1$. This shows that correlated structures are an important effect which is typically comparable to the signal from satellites that are formally inside the halo's virial radius. Our measurements using a fixed 0.15 Mpc cylinder (green box) lie below other measurements for higher values of N_{sats}. This should be unsurprising, since the typical virial radius for our selected halos is roughly 250 kpc. It is interesting to note, however, that the cumulative probability for hosting (at least) one satellite differs by less than 5% when calculated using the virial radius instead of a radius of 150 kpc, while this difference increases rapidly for higher values of N_{sats}. All of these trends indicate the importance of careful background subtraction to eliminate this signal (such as the annulus subtraction of L10), or otherwise of comparing directly to simulations with similar selection criteria so as to properly interpret results.

As concerns the length of our cylindrical aperture, we obtain almost identical results for any length beyond $\sim$ 1Mpc, beyond which the correlation function falls off substantially. Varying the cylinder length from 2−8 Mpc changes our results by roughly five percent, comparable to the size of our statistical errors. Thus, the comparison between satellites defined using our cylindrical aperture and the isotropic background subtraction technique of L10 should be robust.

The numerical values for many of these probabilities — selection by r_{vir}, as well as our cylindrical and fixed spherical apertures — are presented in Table 2. Note that, while we are only counting objects as satellites if they are 2-4 magnitudes dimmer than their hosts for the most accurate comparison with L10, these numbers are essentially identical to considering a threshold sample of objects 0-4 magnitudes dimmer than their (MW-like) hosts. Switching to this definition creates only percent-level changes, well within the statistical error bars.

4.4. *Comparisons Between Simulations and Observations*

Figure 8 and Table 2 show the main result of our analysis, making direct comparison with the results of L10. In the top panel, we compare the L10 $P(N_{sats})$ measurements using their isotropic background subtraction (black asterisks) with our SHAM results using subhalos inside a fixed cylinder with radius 150 kpc and length 5.3 Mpc (blue triangles; cylinder column in Table 2) that closely mimics their selection criteria. The bottom panel shows the comparison between the L10 annulus subtraction (black and gray asterisks) and our measurement of N_{sats} within a 150 kpc spherical aperture (green squares; Sphere column in Table 2). The black and gray asterisks in the lower panel represent the range of measurements based on uncertainty in selecting an optimal background subtraction. The difference between these sets of points thus gives an estimate for the size of the systematic errors in the measurements. Note that, after making their background subtraction, L10 also calculate a systematic adjustment due to catastrophic photo-z failures (see section 4.2 of L10). While we have included those corrections in Figure 8, we have explicitly kept the lower error bar consistent with zero for any measurement that was consistent with zero at the 2-σ level before this systematic correction was included. For reference, Table 2 also gives the $P(N_{sats})$ distribution for proper subhalos, i.e., objects within r_{vir} that are 2-4 magnitudes dimmer than their host.

The agreement between simulations and observations in Figure 8 is generally very good. We take this to indicate a success for both the ΛCDM and SHAM models, particularly indicating, with excellent statistics, that the HOD predicted by Bolshoi for Milky Way-like objects at the massive end matches observations, and there is no evidence for either a missing or excess satellite problem for these objects. Considering our comparison between the cylindrical/isotropic sample, at no N_{sats} do the two results differ by more than $\sim 2.5\sigma$, and in most situations agree to better than 1 σ. The comparison fares slightly worse for the spherical/annulus sample. Here, the simulations underpredicts the number of $N_{sats} = 0$ systems, while over-predicting the $N_{sats} = 1$ systems at the 3 σ level. While this could indicate a real disagreement of the simulation and galaxy formation model with the data at this mass scale, there are a number of other possibilities. First, it is possible that the annulus-subtraction method of L10 overcorrects the background subtraction. This has been tested in simulations, using their algorithm to estimate the number of objects within 150kpc around our halos centers using our

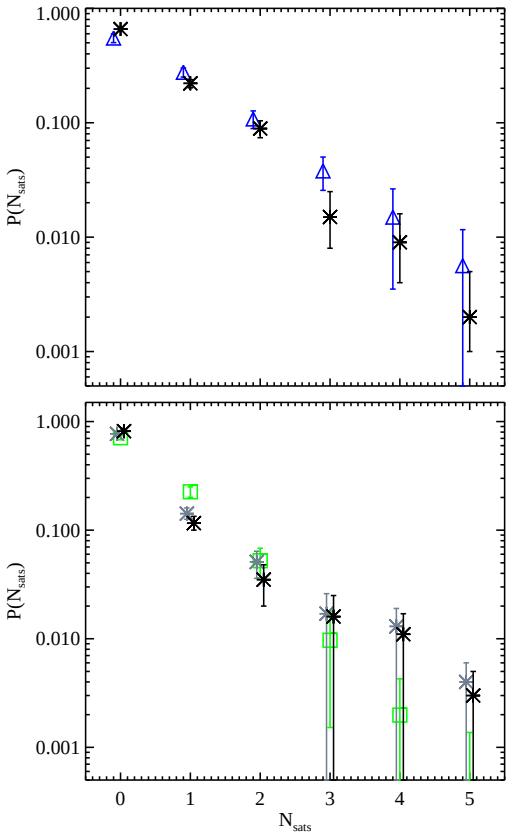

FIG. 8.— Comparisons between the $P(N_{sats})$ distribution of SMC-luminous satellites around MW-luminous hosts in the Bolshoi simulation and the observational results of L10. *Top Panel:* Comparison of the isotropic background subtraction model from L10. Black asterisks represent the abundances from SDSS hosts. The blue triangles denote the abundance of objects inside an aperture that most closely corresponds to the isotropic subtraction model: a fixed cylindrical aperture with radius 150 kpc and length 5.2 Mpc. *Lower Panel:* Same as the upper panel, but now comparing the annulus subtraction model from L10 (black and gray asterisks) to the simulation-equivalent of a fixed 150 kpc spherical aperture for identifying satellite galaxies around their hosts (green squares). For the L10 data, the black points represent our fiducial measurements, while the gray points add a systematic uncertainty to the background subtraction.

TABLE 2
PROBABILITY OF HOSTING N_{sats} SATELLITE GALAXIES BRIGHTER THAN $M_{r,host}+4$ AROUND A MILKY WAY MAGNITUDE HOST HALO WITHIN VARIOUS APERTURES FOR BOTH OUR SIMULATED RESULTS AND THE OBSERVATIONAL MEASUREMENTS FROM L10.

	r^a_{vir}	Cylinder^b	Isotropic^c	Sphere^d	Annulus^c
$P(0)$	$55\pm4\%$	$55\pm5\%$	$66^{+1.6}_{-1.3}$	$71\pm3\%$	$81^{+1.5}_{-1.4}$
$P(1)$	$28\pm3\%$	$28\pm3\%$	$22^{+1.7}_{-1.9}$	$23\pm2\%$	$12^{+1.8}_{-1.6}$
$P(2)$	$11\pm1.4\%$	$11\pm2\%$	$8.9^{+1.5}_{-1.5}$	$5.2\pm1.6\%$	$3.5^{+1.3}_{-1.5}$
$P(3)$	$3.8\pm0.7\%$	$3.8\pm1.2\%$	$1.5^{+1.0}_{-0.7}$	$1.0\pm0.8\%$	$1.6^{+0.9}_{-1.6}$
$P(4)$	$1.55\pm0.4\%$	$1.5\pm1.1\%$	$0.9^{+0.7}_{0.5}$	$0.2\pm0.1\%$	$1.1^{+0.6}_{-1.1}$

[a]halos contained within the virial radius of the host
[b]halos within a cylinder with radius 150 kpc and length 5.2 Mpc
[c]L10 results counting objects within a projected 150 kpc and an isotropic background subtraction
[d]halos within a sphere of radius150 kpc
[e]L10 results counting objects within a projected 150 kpc using an annulus background subtraction

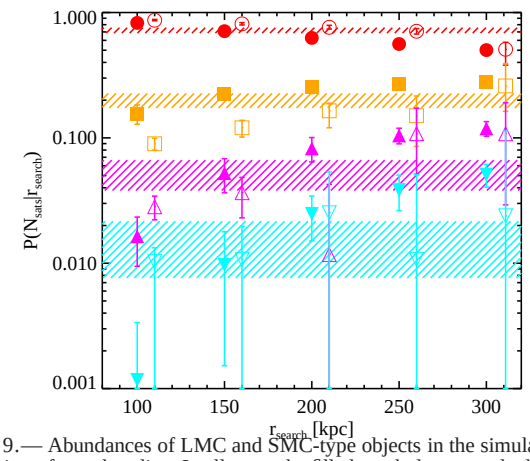

FIG. 9.— Abundances of LMC and SMC-type objects in the simulation, as a function of search radius. In all cases the filled symbols were calculated using Bolshoi+SHAM, while the open symbols represent SDSS measurements from L10. Here, the red circles, orange squares, magenta triangles, and cyan inverse-triangles represent the probability for a Milky Way like galaxy to have 0, 1, 2, or 3 subhalos, respectively. For the Bolshoi objects, the probabilities were calculated using a spherical aperture with varying radius. The SDSS points used the annulus subtraction method of L10. The hatched lines represent the probabilities for hosting N_{sats}subhalos inside the virial radius of the host.

cylindrical counts. The result, is an over preduction of the N_{sats} = 0 term by 6% and an underprediction of the N_{sats} = 1 term by 5%, larger than the estimated systematical uncertainties in Table 1 of L10 (the changes in the higher N_{sats} terms are of similar size to their estimated systematic uncertainty, and are therefore well characterized by the gray points in Figure 8). Such corrections would bring the these terms within 2- and 3- σ of our simulated estimates. It is also important to note that the predictions from simulations depend on the assumed scatter between mass and luminosity. This will be further discussed below.

Looking at the SDSS/Bolshoi comparisons in more detail, we can further investigate the dependence of the $P(N_{sats})$ distribution on the aperture size, as done in L10. For this, we determine the probability of finding N_{sats} satellite galaxies in a spherical aperture around their host, where the radius is varied from 100 to 250 kpc using the annulus background subtraction. The results are shown in Figure 9. Here, the red circles, orange squares, magenta triangles, and cyan inverse-triangles represent the probability of having 0, 1, 2, or 3 subhalos. Open symbols represent SDSS measurements, while filled symbols come from our Bolshoi+SHAM model, while the hatched lines represent the $P(N_{sats})$ distribution for satellites within the virial radius of their hosts. Again, we see good agreement between simulations and observations, although we note the persistence of higher values in the simulation for the N_{sats} = 1 measurement. However, the other values of N_{sats} are in much better agreement.

One of the appeals of the SHAM algorithm is that it has so few free parameters, in this particular case just the scatter (although there are additional implicit assumptions, e.g., about subhalo stripping and star formation after satellite accretion). Figure 10 shows how the scatter impacts this result. Here, we present the probability distribution for an isolated host with M_r = –21.2 to host N_{sats} satellites brighter than –16.5 as we vary the scatter in the SHAM model from 0 to 0.3 dex using our cylindrical method for selecting satellites. While none of

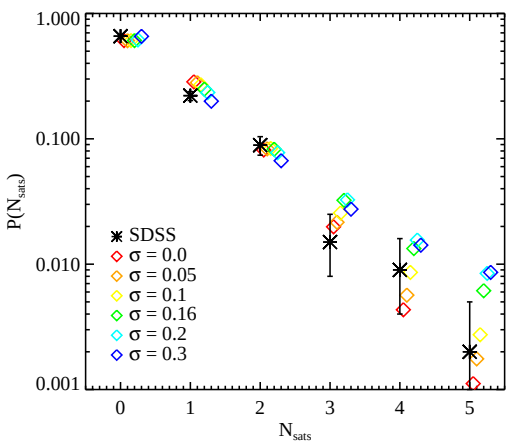

FIG. 10.— Dependence of satellite probabilities on scatter in the relationship between halo mass and galaxy luminosity. Here, we compare the $P(N_{sats})$ distribution calculted using our cylindrical method to the L10 measurements using an isotropic background subtraction. In each case, the model assumes a constant value of σ corresponding to the scatter in log L at a given $v_{\rm acc}$. Larger scatter values tend to have more systems with many satellites, largely because more high mass hosts are scattered into the sample.

these models are ruled out by the data (L10 isotropic model), a number of systematic trends are present. In particular, there is a systematic increase in the probability of hosting 3 or more satellites, along with a decrease in the probability of hosting 1 satellite (by up to 5%). This trend is caused not by scatter in the mass–luminosity relation of the satellite galaxies, but in the mass–luminosity relation of the host objects. As scatter increases, higher and higher mass hosts scatter into our magnitude-selected sample, bringing with them their richer subhalo populations. As we shall discuss in the next section, this has the effect of creating a tail to the negative-binomial distribution that sets the probability for a host to have N_{sats} satellites.

It is also worth noting that the dark blue points representing a scatter of $\sigma = 0.3$ dex look to be violating the trend of an increasing high-N_{sats} probability. This is not due to any special behavior in this regime, but more represents the limits of our simulation resolution. As scatter increases, objects with $M_r - 5\log h > -16.5$, which nominally have $v_{acc} = 90$ km s^{-1}using a scatter-free SHAM, have infall masses as low as 65 km s^{-1}in our $\sigma = 0.3$ dex model. Because tidal stripping can reduce the $v_{\rm max}$ of a subhalo by a factor close to 2 (Wetzel & White 2010; Guo et al. 010), this puts such objects dangerously close to the Bolshoi completeness limit of 50 km s^{-1}. It should be noted, however, that the completeness of subhalos in the Bolshoi simulation is highly dependent on the host mass. Because of stripping of subhalos after accretion, we expect to be losing potentially 10-15% of the satellite population around $\sim 10^{12}h^{-1}{\rm M}_\odot$ mass halos with scatter this high. It's important to appreciate the high resolution necessary to fully model a galaxy population using SHAM. While a scatter of $\sigma = 0.3$ is likely ruled out for massive galaxies (Behroozi et al. 2010b), if such scatter were appropriate the Bolshoi simulation would only be able to populate galaxies down to $M_r \sim -17.5$ while losing fewer than 10% of the objects.

Finally, we should note that there is no compelling reason to assume that both massive and low-mass galaxies exhibit the same scatter in the mass-luminosity relation. We have investigated this by quantifying the variations in the $P(N_{sats})$ distribution where we keep the mass-luminosity scatter of the hosts fixed at 0.16 and vary the scatter of the subhalos from 0-0.3. While we see similar trends with, e.g., the $N_{sats} = 1$ term dropping with increased scatter, the effect is significantly weaker than shown in Figure 10, where we allow the scatter in the host mass-luminosity relation to vary. While it is very possible that the scatter should be even higher than 0.3 for our satellite galaxies, the 50 km s^{-1}resolution limit of Bolshoi prevents us from exploring a wider range. Thus, over the ranger we are able to probe, the scatter in the host mass-luminosity relation, which sets the range of host masses sampled, has a larger impact that the scatter in the satellite mass-luminosity relation.

4.5. *Environmental Effects*

We now revisit the discussion regarding the environmental impact on the subhalo population of §3.2, using observationally motivated environmental measures. Recall that in §3.2, we defined the local environment as the dark matter density in collapsed objects larger than $2 \times 10^{11}{\rm M}_\odot$. Here, we preform a similar analysis using luminosity as an environmental proxy. Specifically, using the isolated central galaxies from our SHAM catalog as selected above, we measure the total luminosity from galaxies brighter than $M_r = -20.8$ (which corresponds to $M_r - 5\log(h) = -20$ in the usual SDSS units) within a sphere of 1 Mpc around our hosts, which we take to be our environment proxy. We then split the sample into our most and least luminous (i.e., dense) quartiles and re-measure the $P(N_{sats})$ distribution for satellites inside their host virial radii. The results are shown in Figure 11. Here, the black points represent the distribution for all isolated hosts, while the red and blue represent those in high/low density environments. As before, we see a clear offset for galaxies in different environments. While the differences are only at the 1-2 sigma levels, high-density halos are systematically more likely to have massive subhalos than those in low density environments. In particular, the underdense halos are 14% more likely to host *no* massive subhalos than their dense counterparts. Similarly, halos in dense environments are twice as likely to host two or more subhalos than those in low density environments. This effect should therefore be an observable manifestation of assembly bias.

5. STATISTICS OF SATELLITES IN LUMINOSITY-SELECTED HOSTS

As noted previously, the inclusion of scatter in the halo $v_{\rm max}$-galaxy luminosity SHAM creates a significant tail in the probability distribution for a host to have N_{sats} satellite galaxies. Consequently, the negative binomial distribution that was found to describe the $P(N_{\rm subs})$ distribution for the subhalos in a mass-selected host does not produce a good fit to $P(N_{\rm sats})$ when applied to luminosity-selected galaxies. Additionally, the change in star formation efficiency with host halo mass breaks the self-similarity that was observed for host halos (Behroozi et al. 2010b, and references therein). In this section, we quantify the $P(N_{sats})$ distribution for satellite galaxies around a luminosity-selected host.

In Figure 12, we show a series of probability distributions for a $M_r = -20.5$ galaxy to host N_{sats} subhalos brighter than -19.8, -18.3 and -16.8 (equivalent to $M_r - 5\log(h) = -19, -17.5, -16$). This plot was generated using a scatter of $\sigma = 0.16$ dex. A low probability tail clearly extends to high N_{sats}. Such a tail was not present when considering $v_{\rm max}$-selected hosts and subhalos in section 3.3. This is emphasized by the dotted lines, which present the negative binomial

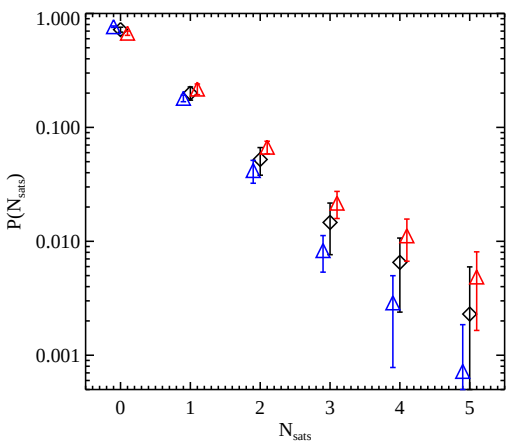

FIG. 11.— The probability distribution for a host galaxy to host *NS* satellites within its virial radius split by environment. The black diamonds represent the distribution for all isolated hosts (and are identical to the black diamonds in Figure 7). The red and blue triangles represent the distribution for hosts in high and low density environments. Here, we use the total luminosity in galaxies brighter than $M_r = -20.8$ as our proxy for density.

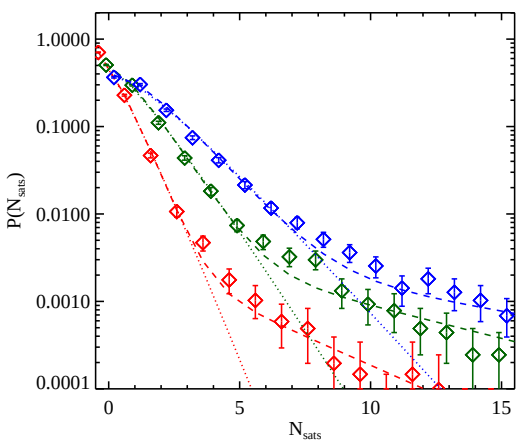

FIG. 12.— Probability of hosting N_{sats} satellite galaxies in a Milky Way-luminosity host, for various satellite selection criteria. The red, green, and blue points represent satellites brighter than $M_r = -19.8, -18.2$, and -16.8. Dotted lines represent the best fit negative binomial distribution, while the dashed line shows the best fit negative binomial plus power-law distribution.

distributions, equation 3, that characterized the $P(N_{subs})$ distribution. While the negative binomial provided an excellent fit to the data for our mass-selected objects, it clearly fails here. While this tail may not appear to be a serious concern, since it is not important until $P(N_{sats}) \sim 1\%$, large surveys such as the SDSS contain more than 10,000 massive clusters, so even these small effects may be visible.

As a better fit, we present a modified binomial distribution by adding a power law tail,

$$P(N|r,p,T,\tau) = \frac{\Gamma(N+r)}{\Gamma(r)\Gamma(N+1)} p^r (1-p)^N + Te^{-\tau N}. \quad (6)$$

Here, the first term is just the negative binomial, with r and p functions of α_2 and $\langle N \rangle$, as defined in Equation 4. The final term models the high-N_{sats} tail that comes about as a result of the $v_{\rm max}$-luminosity scatter, where T and τ control its slope and amplitude. The dashed lines in Figure 12 show the best fits to Equation 6. This clearly provides a significantly improved fit to the simulation measurements, albeit at the expense of adding two new fit parameters. Note, however, that the fit tends to have problems in the cross-over region and that the transition to the high-N_{sats} tail is somewhat more gradual than this model is able to reproduce. While we leave this for future investigations, it is worth noting that changing the scatter in our SHAM model has a direct impact on T and τ. High values of scatter will have a more pronounced tail, which will cause both the amplitude and slope of this tail to increase. For simplicity, for the rest of this work, we will limit ourselves to using a model with $\sigma = 0.16$ dex.

While we could present our best-fitting parameters to the distributions in Figure 12, a much more useful process is to model the $P(N_{sats})$ distribution as a function of both host magnitude and limiting satellite magnitude, as has been done for mass-selected subhalos (see, i.e., Gao et al. 2004). Unfortunately, this proves to be much more difficult for galaxies than for halos. Because the dark matter power spectrum is mostly featureless in the relevant regime, large halos are nearly self-similar versions of smaller halos. As an example of this, the top panel of Figure 3 shows the mean number of satellites above a given mass cut for mass-selected host halos. This distribution exhibits a power-law behavior with nearly identical parameters regardless of the host mass. This is not the case for magnitude-selected objects.

Figure 13 presents the best-fit parameters for the satellite $P(N_{sats})$ distribution as modeled by Equation 6 around galaxies as a function of limiting subhalo luminosity (i.e., magnitude difference). The red, orange, yellow, dark green, green, and blue points represent hosts with $M_r = -20.3, -20.8, -21.3, -21.8, -22.3$, and -22.8. As can be clearly seen in the top left panel, which shows the trend of the mean number of satellite galaxies ($\langle N \rangle$) with luminosity ratio, galaxies do not scale self-similarly. At a given luminosity ratio, brighter galaxies are significantly more likely to have a larger N_{sats} (expected number of satellites) than dimmer galaxies.

This is a manifestation of the varying star formation efficiency with halo mass as seen in, e.g., Figure 4. For masses above 10^{12} $M_\odot$, star formation efficiency becomes less efficient, so the rate of increase of M_r with v_{max} is shallow. At masses lower than 10^{12} $M_\odot$, star formation efficiency drops rapidly with decreasing mass, leading to a much steeper rate of change of M_r with respect to v_{max}. Thus, for a fixed bin in M_r, the corresponding logarithmic range in v_{max} will be much less for low-mass galaxies as compared to high-mass galaxies. As such, while the $\langle N \rangle$ values for mass-selected subhalos lie on a single line in Figure 3, luminosity-selected halos do not scale in such a manner, resulting in the different lines in the top-left panel of Figure 13: brighter host galaxies have more satellites at a fixed luminosity ratio, L_{sat}/L_{host}, than dimmer hosts.

A number of the trends present in Figure 13 can be readily understood in terms of simple models. As discussed above, the behavior of $\langle N \rangle$ is simply a manifestation of the changing star formation efficiency with halo mass. Similarly, the trends in τ can be understood though simple scaling relations. First, consider a fixed luminosity ratio, $|M_{r,host} - M_{r,lim}|$. Since brighter hosts correspond to more massive halos, these objects live in a steeper part of the mass function, where a fixed scatter creates a broader selection of host masses, the larger of which are more likely to host bright satellites. Because of this, the exponential tail falls off more slowly, resulting in a

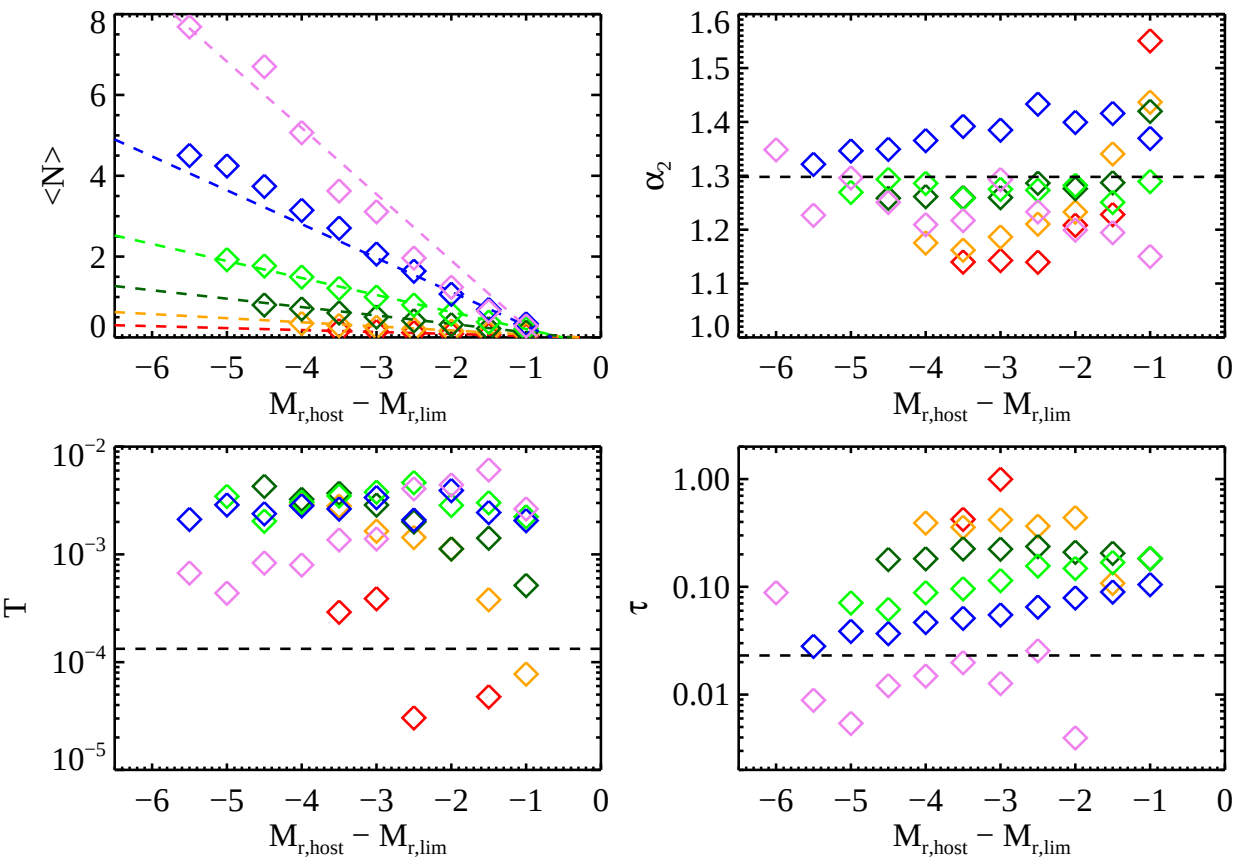

FIG. 13.— The fit parameters specifying the P(N) distribution (equation 6) as a function limiting satellite magnitude, represented as a magnitude difference (luminosity ratio) Different colored points represent different host populations: violet, blue, green, dark green, orange, and red points are hosts with M_r = –19.8, –20.3, –20.8, –21.3, –21.8, and –22.3. Dashed lines represent out fits to these distributions, as given in Equation 7.

lower τ. The trend of τ increasing with luminosity ratio for a fixed host mass.

Guided by these observations, and noting that α_2 and T don't have strong trends with either host magnitude or limiting luminosity ratio, we propose a 7-parameter fit to generally describe the full $P(N|M_{r,host}, M_{r,lim})$. We use our generalized negative-binomial plus power law as defined in Equation 6, and keep α_2, T, and τ constant. However, we parameterize $\langle N \rangle$ as a linear function, the slope of which depends on $M_{r,host} - M_{r,lim}$ and the offset of which depends on host magnitude, $M_{r,host}$. Our full fit for Equation 6 then becomes a function of the parameters $N_{0.a}, N_{0,b}, N_{1,a}, N_{1,b}, \alpha_2, T_0$, and τ_0 defined by:

$$P(N|M_{r,host}, M_{r,lim}) = \frac{\Gamma(N+r)}{\Gamma(r)\Gamma(N+1)} p^r (1-p)^N + T_0 e^{-\tau_0 N} \quad (7)$$

where

$$p = \frac{1}{1+(\alpha_2^2-1)\langle N \rangle (M_{r,host}, M_{r,lim})}$$
$$r = \frac{1}{\alpha_2^2 - 1} \quad (8)$$
$$\langle N \rangle (M_{r,host}, M_{r,lim}) = -10^{N_{0,a}+N_{0,b}*\log(-M_{r,host}+5\log(h))} - (M_{r,host} - M_{r,lim}) 10^{N_{1,a}+N_{1,b}*\log(-M_{r,host}+5\log(h))}.$$

We fit this functional form to the measured $P(N_{sats})$ distribution for all host halos down to $M_r = -18.5$ and their satellites down to $M_r = -16$ in Bolshoi stacked in bins of 0.5 mag. We present our best fitting parameters for Equation 8 in table 5. As a final validation of this result, Figure 14 shows the measured $P(N)$ distributions for a range of $M_{r,host}$ and $M_{r,lim}$, along with the fits from our model in Eq. 7. Note that, because the slope and intercept of $\langle N \rangle (M_{r,host}, M_{r,lim})$ are linear functions in log space, the exact value of $\langle N \rangle$ is highly sensitive to the parameters $N_{0,a}, N_{0,b}, N_{1,a}$, and $N_{1,b}$. Because of this, it is necessary to constrain these parameters to 4 significant figures (which is easily done given the constraints from the Bolshoi simulation).

While our nominal fit can be improved using a τ that is a power-law in $M_{r,host} - M_{r,lim}$ with a normalization that depends on host mass, the actual fit does not significantly improve the reduced χ^2, so we elect to hold it constant.

TABLE 3
PARAMETERS SPECIFYING $P(N)$ DISTRIBUTION IN EQ. 8

parameter	best-fit value
$N_{0,a}$	-53.70
$N_{0,b}$	40.11
$N_{1,a}$	-39.05
$N_{1,b}$	29.25
α_2	1.3
T_0	1.3×10^{-4}
τ_0	0.023

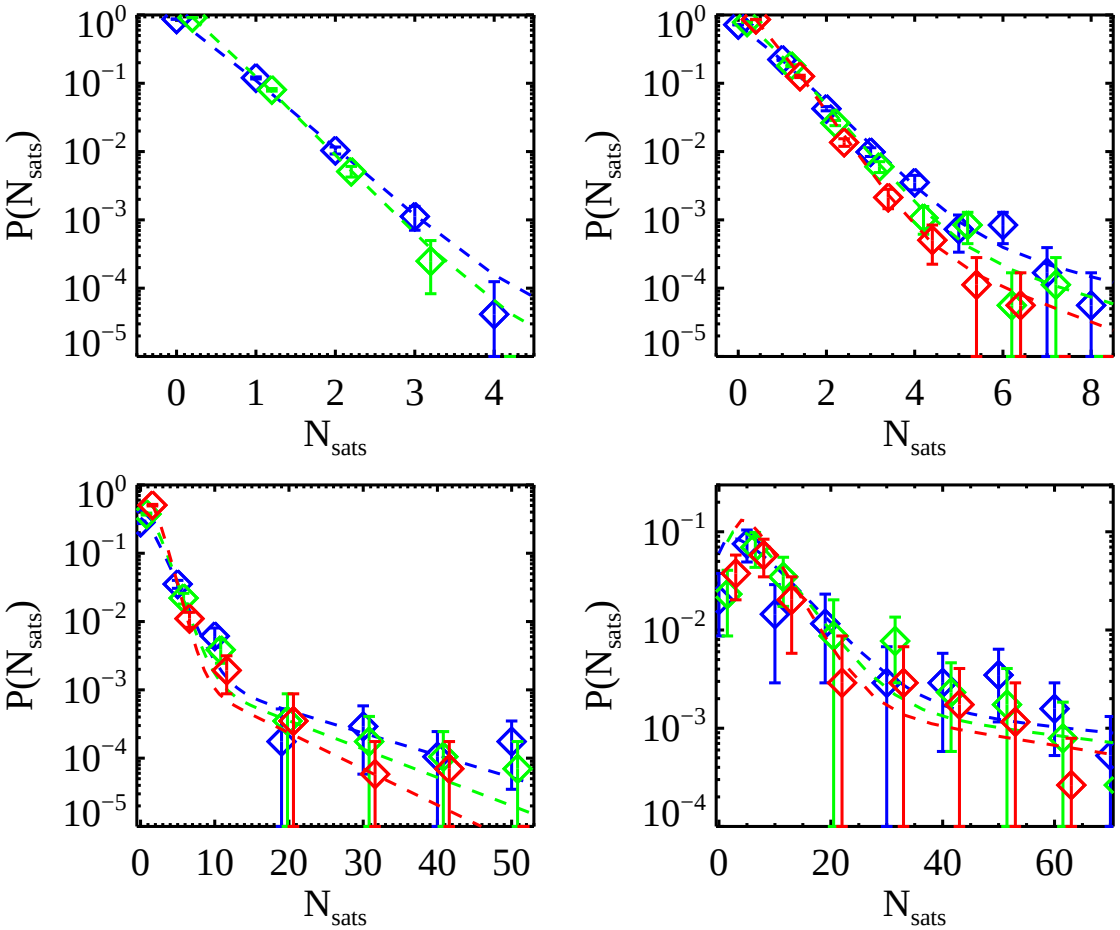

FIG. 14.— Probability distributions for galaxies to host N_{sats} satellites (diamonds). The four panels represent different selections based on host magnitudes $M_{r,host} = -19.5, -20.5, -21.5, -22.5$ for the top left through lower right. The blue, green, and red points represent various limiting satellite magnitudes, $M_{r,lim} = -16.5, -17.5, -18.5$. The dashed lines represent our model with fit parameters from Eq. 7 and Table 5.

6. CONCLUSIONS AND SUMMARY

In this work, we have examined the likelihood for simulated MW-like dark matter halos to host substructures similar to the Magellanic Clouds. We have performed this analysis using both dark matter kinematic information and an abundance-matching technique which assigns galaxy luminosities to resolved dark matter halos and allows direct comparison with observations (e.g., L10). The main result of this work is that MW-like objects have a 5-11% chance to host two subhalos as large or as luminous as the SMC, in basic agreement with previous simulation results (e.g., BK10), as well as with observations. While we have extensively compared our results for the full probability distribution for a MW-luminous galaxy to host N_{sats} satellite galaxies to the observational measurements from L10, finding good agreement. This results are also in qualitative agreement with previous results using smaller samples (Chen et al. 2006; James & Ivory 2010).

Our results have a number of implications. First, this is a validation of the ΛCDM paradigm down to the level of $10^{10}h^{-1}\mathrm{M}_{\odot}$ objects. At this level, there is no indication that either the CDM paradigm or our standard picture of galaxy formation, including the relatively tight relationship between galaxy luminosities and halo masses, breaks down. In particular, it appears that the statistics of satellite galaxies at this mass in LCDM are in very good agreement with observations which sample a wide range of galaxy environments.

One possible criticism of the model we have used for connecting galaxies to halos (SHAM) is that it may be so robust as to *always* reproduce the observed statistics, given its assumption of the correct global luminosity function. In order to evaluate this, it is important to keep track of the exact assumptions of the approach and how these relate to the particular statistics measured. First and foremost, SHAM assumes that v_{max} of a halo or subhalo (at accretion into a larger system) is the *only* parameter that sets the luminosity of the galaxy it hosts. While this is robust to, e.g., a temporally-variable star formation efficiency with halo mass, it would differ from model in which there was environmental dependence to the galaxy formation recipe in addition to the inherent environmental dependence of the halo mass function. For example, if subhalos of a given mass evolve very differently than halos of the same mass in the field, our model would not produce good agreement. Additionally, if our simulated dark matter halo mass function was significantly off from reality (due to, for example, an incorrect σ_8 or Ω_m), the masses of the MCs as estimated from abundance matching would not provide a good match to the direct kinematic measurements, as we find here. Finally, this is a test of the SHAM treatment of subhalos

in a mass regime lower than has been previously explored.

We do see some manifestations of assembly bias with regard to the dark matter subhalo population inside MW-like galaxies: halos in higher density regions host more massive subhalos than those in lower density regions. This effect appears to be most pronounced for relatively local measurements of density, and suggests that the MW's proximity to M31 boosts the likelihood for us to see a LMC/SMC pair by about 25%. The effect is strongest for densities measured on the scale of 1 Mpc. We note that such a boost seems to be present if we use either the total local mass or the total local luminosity as an environmental measure. This should make the effect an observable manifestation of assembly bias (though detecting it will require careful treatment of correlated structure). It is interesting that this result is in qualitative agreement with the work of Ishiyama et al. (2009b), who saw a similar trend with environment but claimed it was most sensitive at the $\sim 5h^{-1}$Mpc scale. They note that we are in an underdense region on these scales, and cite this as a possible ingredient for solving the missing satellite problem. While our simulations do not allow us to determine the probabilities of finding objects smaller than the Magellanic Clouds, if our observed trend were extrapolated down to lower masses it would result in an *opposite* effect, where the presence of M31 could serve to exacerbate the missing satellite problem.

Finally, we have generalized our measurements for the $P(N_{sats})$ distribution over a wide range of host and satellite luminosities. Our results show a significant deviation from the Poisson expectation for larger values of N_{sats}. While these deviations are typically present only in the low-likelihood tail of the distribution, the large volume of surveys like SDSS should allow tests of these predictions with observations. Deviations from Poisson statistics in the number of satellites may also have consequences for HOD modeling, which currently assume a Poisson distribution for the number of galaxies given the halo mass.

RHW and MTB were supported by the National Science Foundation under grant NSF AST-0908883. RHW, PSB, and BFG received support from the U.S. Department of Energy under contract number DE-AC02-76SF00515. AK and JRP were supported by NASA ATP and NSF AST grants. The Bolshoi simulation was run on the NASA Advanced Supercomputing (NAS) Pleiades computer at NASA Ames Research Center. We thank Louie Strigari, Lulu Liu, and Anna Nierenberg for useful discussions.

REFERENCES

Abazajian, K. N., Adelman-McCarthy, J. K., Agüeros, M. A., Allam, S. S., Allende Prieto, C., An, D., Anderson, K. S. J., Anderson, S. F., Annis, J., Bahcall, N. A., & et al. 2009, ApJS, 182, 543
Battaglia, G., Helmi, A., Morrison, H., Harding, P., Olszewski, E. W., Mateo, M., Freeman, K. C., Norris, J., & Shectman, S. A. 2005, MNRAS, 364, 433
Behroozi, P. S., Busha, M., Wechsler, R. H., et al. 2010a, in preparation
Behroozi, P. S., Conroy, C., & Wechsler, R. H. 2010b, ApJ, 717, 379
Besla, G., Kallivayalil, N., Hernquist, L., Robertson, B., Cox, T. J., van der Marel, R. P., & Alcock, C. 2007, ApJ, 668, 949
Blanton, M. R. & Roweis, S. 2007, AJ, 133, 734
Blanton, M. R., Schlegel, D. J., Strauss, M. A., Brinkmann, J., Finkbeiner, D., Fukugita, M., Gunn, J. E., Hogg, D. W., Ivezić, Ž., Knapp, G. R., Lupton, R. H., Munn, J. A., Schneider, D. P., Tegmark, M., & Zehavi, I. 2005, AJ, 129, 2562
Blanton, M. R. et al. 2003, ApJ, 592, 819
Blumenthal, G. R., Faber, S. M., Primack, J. R., & Rees, M. J. 1984, Nature, 311, 517
Boylan-Kolchin, M., Springel, V., White, S. D. M., & Jenkins, A. 2010, MNRAS, 406, 896
Boylan-Kolchin, M., Springel, V., White, S. D. M., Jenkins, A., & Lemson, G. 2009, MNRAS, 398, 1150
Busha, M. T., Evrard, A. E., & Adams, F. C. 2007, ApJ, 665, 1
Busha, M. T., Marshall, P. J., Wechsler, R. H., Klypin, A., & Primack, J. 2010, ArXiv e-prints, arXiv:1011.2203
Chen, J., Kravtsov, A. V., Prada, F., Sheldon, E. S., Klypin, A. A., Blanton, M. R., Brinkmann, J., & Thakar, A. R. 2006, ApJ, 647, 86
Conroy, C., Wechsler, R. H., & Kravtsov, A. V. 2006, ApJ, 647, 201
Dehnen, W., McLaughlin, D. E., & Sachania, J. 2006, MNRAS, 369, 1688
Diemand, J., Moore, B., & Stadel, J. 2004, MNRAS, 352, 535
Evrard, A. E., Bialek, J., Busha, M., White, M., Habib, S., Heitmann, K., Warren, M., Rasia, E., Tormen, G., Moscardini, L., Power, C., Jenkins, A. R., Gao, L., Frenk, C. S., Springel, V., White, S. D. M., & Diemand, J. 2008, ApJ, 672, 122
Gao, L., Frenk, C. S., Boylan-Kolchin, M., Jenkins, A., Springel, V., & White, S. D. M. 2010, ArXiv e-prints, arXiv:1006.2882
Gao, L., White, S. D. M., Jenkins, A., Stoehr, F., & Springel, V. 2004, MNRAS, 355, 819
Gnedin, O. Y., Brown, W. R., Geller, M. J., & Kenyon, S. J. 2010, ApJ, 720, L108
Guo, Q., White, S., Li, C., & Boylan-Kolchin, M. 2010, MNRAS404, 1111G
Harris, J. & Zaritsky, D. 2006, AJ, 131, 2514
Ishiyama, T., Fukushige, T., & Makino, J. 2009a, ApJ, 696, 2115
—. 2009b, ApJ, 696, 2115
James, P. A. & Ivory, C. F. 2010, ArXiv e-prints, arXiv:1009.2875
Kallivayalil, N., van der Marel, R. P., & Alcock, C. 2006a, ApJ, 652, 1213
Kallivayalil, N., van der Marel, R. P., Alcock, C., Axelrod, T., Cook, K. H., Drake, A. J., & Geha, M. 2006b, ApJ, 638, 772
Klypin, A. & Holtzman, J. 1997, ArXiv Astrophysics e-prints, arXiv:astro-ph/9712217
Klypin, A., Kravtsov, A. V., Valenzuela, O., & Prada, F. 1999, ApJ, 522, 82
Klypin, A., Trujillo-Gomez, S., & Primack, J. 2010, ArXiv e-prints, arXiv:1002.3660
Komatsu, E. et al. 2010, ArXiv e-prints, arXiv:1001.4538
Koposov, S. E., Yoo, J., Rix, H., Weinberg, D. H., Macciò, A. V., & Escudé, J. M. 2009, ApJ, 696, 2179
Kravtsov, A. V., Berlind, A. A., Wechsler, R. H., Klypin, A. A., Gottlöber, S., Allgood, B., & Primack, J. R. 2004, ApJ, 609, 35
Kravtsov, A. V., Klypin, A. A., & Khokhlov, A. M. 1997, ApJS, 111, 73
Lacey, C. & Cole, S. 1993, MNRAS, 262, 627
Li, Y., Helmi, A., De Lucia, G., & Stoehr, F. 2009, MNRAS, 397, L87
Libeskind, N. I., Cole, S., Frenk, C. S., Okamoto, T., & Jenkins, A. 2007, MNRAS, 374, 16
Liu, L., Gerke, B. F., Wechsler, R. H., Behroozi, P. S., & Busha, M. T. 2010, ArXiv e-prints, arXiv:1011.2255
Madau, P., Diemand, J., & Kuhlen, M. 2008, ApJ, 679, 1260
Marín, F. A., Wechsler, R. H., Frieman, J. A., & Nichol, R. C. 2008, ApJ, 672, 849
Moore, B., Ghigna, S., Governato, F., Lake, G., Quinn, T., Stadel, J., & Tozzi, P. 1999, ApJ, 524, L19
More, S., van den Bosch, F. C., Cacciato, M., Mo, H. J., Yang, X., & Li, R. 2009, MNRAS, 392, 801
Okamoto, T., Frenk, C. S., Jenkins, A., & Theuns, T. 2010, MNRAS, 406, 208
Smith, M. C. et al. 2007, MNRAS, 379, 755
Springel, V., Wang, J., Vogelsberger, M., Ludlow, A., Jenkins, A., Helmi, A., Navarro, J. F., Frenk, C. S., & White, S. D. M. 2008, MNRAS, 391, 1685
Springel, V., White, S. D. M., Tormen, G., & Kauffmann, G. 2001, MNRAS, 328, 726
Stadel, J., Potter, D., Moore, B., Diemand, J., Madau, P., Zemp, M., Kuhlen, M., & Quilis, V. 2009, MNRAS, 398, L21
Stanimirović, S., Staveley-Smith, L., & Jones, P. A. 2004, ApJ, 604, 176
Tasitsiomi, A., Kravtsov, A. V., Wechsler, R. H., & Primack, J. R. 2004, ApJ, 614, 533
Trujillo-Gomez, S., Klypin, A., Primack, J., & Romanowsky, A. J. 2010, ArXiv e-prints, arXiv:1005.1289
van den Bergh, S. 2000, The Galaxies of the Local Group (Cambridge)
van der Marel, R. P., Alves, D. R., Hardy, E., & Suntzeff, N. B. 2002, AJ, 124, 2639

Wechsler, R. H., Bullock, J. S., Primack, J. R., Kravtsov, A. V., & Dekel, A. 2002, ApJ, 568, 52
Wetzel, A. R. & White, M. 2010, MNRAS, 403, 1072
Xue, X. X., Rix, H. W., Zhao, G., Re Fiorentin, P., Naab, T., Steinmetz, M., van den Bosch, F. C., Beers, T. C., Lee, Y. S., Bell, E. F., Rockosi, C., Yanny, B., Newberg, H., Wilhelm, R., Kang, X., Smith, M. C., & Schneider, D. P. 2008, ApJ, 684, 1143
York, D. G. et al. 2000, AJ, 120, 1579
Zehavi, I., Zheng, Z., Weinberg, D. H., Blanton, M. R., Bahcall, N. A., Berlind, A. A., Brinkmann, J., Frieman, J. A., Gunn, J. E., Lupton, R. H., Nichol, R. C., Percival, W. J., Schneider, D. P., Skibba, R. A., Strauss, M. A., Tegmark, M., & York, D. G. 2010, ArXiv e-prints, arXiv:1005.2413
Zentner, A. R., Berlind, A. A., Bullock, J. S., Kravtsov, A. V., & Wechsler, R. H. 2005, ApJ, 624, 505
Zentner, A. R. & Bullock, J. S. 2003, ApJ, 598, 49